PAPER

Cold shock induces apoptosis of dorsal root ganglion neurons plated on infrared windows

Ebrahim Aboualizadeh,[a] Eric C. Mattson,[a] Crystal L. O'Hara,[b] Amanda K. Smith,[b] Cheryl L. Stucky[b] and Carol J. Hirschmugl*[a]

The chemical status of live sensory neurons is accessible with infrared microspectroscopy of appropriately prepared cells. In this paper, individual dorsal root ganglion (DRG) neurons have been prepared with two different protocols, and plated on glass cover slips, BaF_2 and CaF_2 substrates. The first protocol exposes the intact DRGs to 4 °C for between 20–30 minutes before dissociating individual neurons and plating 2 hours later. The second protocol maintains the neurons at 23 °C for the entire duration of the sample preparation. The visual appearance of the neurons is similar. The viability was assessed by means of trypan blue exclusion method to determine the viability of the neurons. The neurons prepared under the first protocol (cold exposure) and plated on BaF_2 reveal a distinct chemical signature and chemical distribution that is different from the other sample preparations described in the paper. Importantly, results for other sample preparation methods, using various substrates and temperature protocols, when compared across the overlapping spectral bandwidth, present normal chemical distribution within the neurons. The unusual chemically specific spatial variation is dominated by a lack of protein and carbohydrates in the center of the neurons and signatures of unraveling DNA are detected. We suggest that cold shock leads to apoptosis of DRGs, followed by osmotic stress originating from ion gradients across the cell membrane leading to cell lysis.

Introduction

Isolated, individual cells from animals or native tissues (*e.g.*, neurons, stem cells, breast cells) are ideal for detecting biochemistry and morphology *via* a variety of imaging approaches namely, fluorescence with fluorescent tags, infrared for chemical imaging, electrophysiology with patch clamp techniques, calcium imaging using calcium sensitive dyes or genetically encoded calcium sensors, and atomic force microscopy. While identical cell preparation (*e.g.* dissociation methods, incubation approaches, choice of substrates) would be ideal for all of these studies, each technique has unique requirements. In particular, a distinct combination of molecular and cellular properties of DRG sensory neurons have been elucidated in primary DRG cultures.[1–8] However, because individual neurons are often dissociated from the whole ganglion in order to conduct single cell patch clamp recordings or calcium imaging, there are several steps in the process that could cause damage to the neurons. First, the peripheral and central axons

are cleaved from the DRG, resulting in "axotomized" somata. Second, collagenase and trypsin are used to chemically dissociate the ganglia, and they act by partially digesting the extracellular matrix and can cleave proteins from the membrane surface.[9] Third, enzyme-treated ganglia are then mechanically triturated through a restricted opening in a pipette to produce single-cell suspensions. This can mechanically cleave proteins from the cell surface or cause damage. If the tissue is exposed to the enzymes too long or triturated too hard or fast, the cells could be damaged and subsequently undergo cell death.[9]

Based on both morphological and functional criteria, DRG neurons isolated from adult mice can be classified into large-diameter (≥27 μm) and small-diameter (<27 μm) somata. DRG neurons with large somata tend to have myelinated Aα and Aβ axons *in vivo*[10] and generally conduct proprioceptive or mechanical information from peripheral targets at high velocities. DRG neurons with small to medium-diameter somata tend to correspond *in vivo* to unmyelinated C fibers and Aδ fibers. Many of the small diameter DRG neurons are nociceptive, or pain-sensing[11–13] or thermosensors and conduct information from pain and thermal receptors at low velocities.[14] A further population of small neurons is low-threshold C fibers that convey gentle touch and skin stroke.[15]

[a]*Department of Physics, University of Wisconsin-Milwaukee, Milwaukee, WI, 53211 USA. E-mail: cjhirsch@uwm.edu; Tel: +1 (414) 229-5748*
[b]*Department of Cell Biology, Neurobiology and Anatomy, Medical College of Wisconsin, Milwaukee, WI, 53226-0509 USA*

Fourier transform infrared (FTIR) widefield microscopy provides label-free imaging that detects the distribution of biologically relevant components in cells, concurrently revealing biochemical composition and morphology of the cells.[16] Lipids and carbohydrates that are readily detected with mid-infrared radiation have been shown to modulate the properties of mechanotransduction in cells.[17] For example, disruption of lipid rafts decreases mechanical sensitivity of osteoblasts and epithelial cells.[18–20] Membrane phospholipids have been shown to modulate mechanical properties of sensory neurons.[21] Mid-infrared measurements require proper substrate choice and sufficient specimen thickness based on sampling modes. Biological tissues and individual cells are typically measured in transmission mode using infrared transparent calcium fluoride (CaF_2) or barium fluoride (BaF_2) substrates. The transmission bandwidth for BaF_2 window is broader than CaF_2 and includes absorption bands from important functional groups for carbohydrates (1200–1000 cm^{-1}). CaF_2 has a rapidly changing dielectric response in this spectral range, affecting the ability to properly focus the optics for broadband microscopy to concurrently measure all wavelengths.[22] Diamond is inert, has a constant index of refraction over a broad bandwidth for excellent optical properties, but is comparatively expensive. Glass is a typical substrate for cells and tissues for visible light studies and many experiments in the lab (e.g., patch clamp, calcium imaging), but absorbs across a portion of the mid-IR spectral range. A low cost alternative in many cases is to measure in transflection geometry, measuring the transmission through a sample mounted on a mid-IR reflective surface, gold-coated disc or indium tin oxide covered slides. Absorption intensities are proportional to the sample thickness in transmission, and are twice the strength for transflection versus transmission for the same sample.[23] However, for transflection the samples in this case must be much thinner than the wavelength of light (2–10 micrometers) due to the varying intensity of the infrared field perpendicular to the surface on this scale.[24,25] In the present study, infrared transmission measurements of DRGs cultured on a CaF_2 substrate (well-recognized biocompatible substrate to BaF_2), BaF_2 (chosen for the best tradeoff between largest bandwidth and lowest cost) and glass coverslips (for measurements of traditionally prepared neurons, but with limited bandwidth) are compared. The chemical status of the DRG neurons was compared for the overlapping spectral bandwidth facilitating a statistically based comparison of the chemical status of the cells on these two substrates.

Materials and methods

Animals

Experiments were conducted on male C57BL/6J mice (wild-type), aged 3–6 months (Jackson Laboratories).[26] The Institutional Animal Care and Use Committee of the Medical College of Wisconsin approved all experimental procedures.

Coating substrates with laminin

All the experiments in this work used laminin-coated BaF_2, CaF_2 and glass coverslip substrates to promote cell adhesion. Substrates were placed in 6 well plates. Laminin was then added to the substrates. The laminin solution was prepared by dissolving 1 mg ml^{-1} laminin in 500 μl of phosphate-buffered saline (PBS). The solution was then added to each individual substrate. The substrates were incubated for two hours at 37 °C; the laminin was then removed and was allowed to dry. Cell suspension was added immediately after the coating dried. The DRG neurons adhered better to glass than to BaF_2 and CaF_2 windows based on more neurons plating for longer time period.

DRG culture

Lumbar DRGs were cultured as previously described[27,28] and summarized here. For the purpose of this study, the neurons were dissected after maintaining intact DRG aggregates at two different temperatures: (i) 4 °C ± 2 °C and (ii) 23 °C ± 2 °C. In the former case, the intact DRGs were maintained in an ice bath for up to 20–30 minutes at 4 °C. The neurons were then dissociated and plated 2 hours later as described in ref. 29. In the latter case the intact DRGs were maintained at room temperature (23 °C) during the preparation, from dissecting out of animal until plating to the window. After the dissociated DRGs were plated onto laminin-coated substrates, they were incubated for 2 hours at 37 °C and 5% CO_2 to allow adherence and no exogenous growth factors were added. Windows were then flooded with DMEM/Hams-F12 medium supplemented with 10% heat-inactivated horse serum, 2 mM L-glutamine, 0.8% D-glucose, 100 units penicillin and 100 μg ml^{-1} streptomycin. Chemical imaging experiments were conducted 18–24 hours after the neurons were plated to be consistent with the time range when many patch-clamp and calcium imaging recordings have been performed.[27,30,31] Cultures were transported in humidified Petri dishes. At least three independent primary culture preparations were conducted from three different wild-type naïve mice.

FTIR widefield microscopy

FTIR widefield microscopy detects biologically relevant functional groups. The samples are evaluated with a Bruker Vertex 70 IR Microscope and a Bruker Hyperion 3000 IR Microscope equipped with a thermal blackbody source. The focal plane array (FPA) detector is a multielement detector (128 × 128 pixels) coupled with the interferometer to collect hyperspectral data sets (x, y, Abs(λ)). The measurements were performed using a 36× Cassegrain microscope objective (numerical aperture 0.5) and a 15× aperture objective (N.A 0.4). With this experimental geometry, the effective geometric pixel size at the sample plane is 1.1 × 1.1 μm^2. The data were collected with 128 co-added scans at 8 cm^{-1} spectral resolution. Data were acquired using OPUS 6.5 software (Bruker) and analyzed using IRidys.[32]

Initially, a background measurement was collected from an area of the laminin-coated substrate, which is a thin layer of laminin. A sample measurement is ratioed to this background measurement to determine the quantity of light that is absorbed by the sample. The laminin is distributed homogeneously on the window in order to improve the cell adhesion. We measured the background on a laminin-coated area of the window. We conclude that at most 4% of the absorption could be affected by the absorptions due to laminin (data not shown). The neurons adhere to the window; the window is removed from the medium, and left to dry for 20 minutes at room temperature. There is no fixation applied to the cells prior to FTIR imaging.

Chemical images and average spectra were analyzed on each substrate for different subpopulations of sensory neurons. Chemically specific images were generated by calculating the area under a given characteristic peak for every pixel of the field of view, and the results are displayed as false-colored images using a rainbow color scale (blue/red low/high absorption intensity). Average spectra for a given cell were calculated by defining a region of interest (ROI) such that only the pixels comprising the area occupied by the cell were included in the averaging. Since the fingerprint region (1500 cm^{-1}–1000 cm^{-1}) could not be evaluated in the spectra when using glass coverslips as a substrate, the overlapping mid-IR spectral region (3800–1500 cm^{-1}) was used for the statistical data analysis. This region includes functional groups from most of the biologically relevant molecules such as proteins, lipids, carbohydrates and water, which allows a fair comparison between these substrates. Two thermal conditions during sample preparation are considered for each substrate, to confirm or refute whether changes in neuron chemical status and morphology are sample preparation or substrate dependent.

Results and discussion

Since small and large diameter (*i.e.* small-diameter (<27 μm)) and large-diameter ((≥27 μm) somata) sensory neurons have generally different functions in the somatosensory system, they were divided into subpopulations to facilitate comparisons of more homogeneous cell populations, although even within these two basic subpopulations there is also considerable biological heterogeneity. Thus, datasets consisting of many small diameter (SD) or large diameter (LD) individual neurons from different subpopulations from three naïve C57BL/6J (wild-type) mice were compared to reveal biological variations due to sample preparation.

Viability test

The Trypan Blue exclusion method was employed (trypan blue solution 0.4%) to assess the cell viability on BaF_2 substrate and differentiate between viable and non-viable cells. Viability test showed that 96% of the neurons that are maintained at 23 °C and plated on BaF_2 substrate were viable (160 neurons

were counted). For the neurons that are maintained at 4 °C and plated on the BaF_2 window only 23% of the neurons were viable (180 neurons were counted). The reduced viability for the latter protocol is completely in agreement with our findings from infrared microspectroscopy, which will be discussed in the next section. In contrast, the viability of the neurons maintained at 4 °C and plated on glass coverslip was assessed and 90% of the cells were viable (150 neurons were counted).

Infrared spectra and chemical images of representative sensory neurons

Hyperspectral data is displayed in Fig. 1 and 2 for representative individual LD and SD neurons, respectively. Chemical images from neurons obtained from intact DRGs maintained at 4 °C (panels B–F, L–O, T–U) *vs.* 23 °C (panels G–K, P–S, V–W) and plated on BaF_2 (panels B–K), CaF_2 (panels L–S) and glass (panels T–W) are shown. Average spectra are shown in Fig. 1 and 2 panel A, identifying the infrared bands associated with the vibrations of the major functional groups of proteins, hydrocarbons, carbohydrates and phosphates. The infrared bands, for the overlapping transparent ranges for the windows, include: 2800–3000 cm^{-1} (C–H stretching of hydrocarbons, primarily lipids) and 3000–3600 cm^{-1} (that has contributions from N–H stretching modes of proteins and stretching modes from carbohydrates). Additional absorption bands for C=O stretching of amide functional groups in protein (1600–1700 cm^{-1}), asymmetric stretching of phosphates (1188–1280 cm^{-1}) and the spectral range 1010–1166 cm^{-1}, which has stretching mode of carbohydrates, nucleic acid modes and the symmetric stretching of phosphate moieties are observed with the broad spectral range for the CaF_2 and BaF_2 windows. The chemical images derived from integrating the absorption band for each functional group for LD (Fig. 1) and SD (Fig. 2) neurons are shown. Chemical images reveal the relative concentrations of each functional group on a rainbow color scale, (red (blue)/highest (lowest) intensity) to correspond to the absorption intensity and therefore concentration. Visible images of the LD and SD neurons on all three optical substrates were considered identical, not revealing any obvious differences.

Large diameter DRG neuron chemistry and morphology

First, consider the FTIR measurements for LD neurons that were maintained at 4 °C at the intact DRG stage, and plated on glass coverslips (Fig. 1 panels T–U), similar to the sample preparation for the patch clamp and calcium imaging experiments in the lab.[27,30] In this case, one neuron is in the field of view. The blue background clearly denotes the lack of biological material, while the green to red distributions show elevated levels. Note that the protein distribution is throughout the neuron, with the remaining chemical images showing maxima in the center of the neuron and less homogeneity.

Next, to have access to a broader, more informative spectral range, the chemical images of the LD neurons obtained from intact DRGs maintained at 4 °C and plated on BaF_2 (Fig. 1 panels B–F) are evaluated. These images show that the N–H/O–
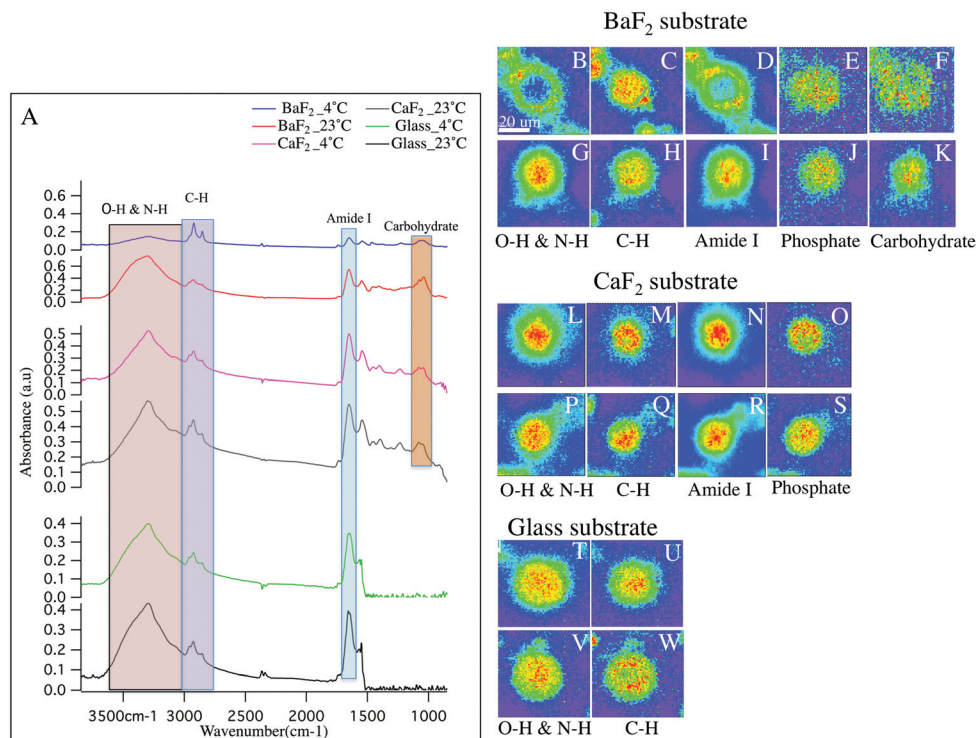
Fig. 1 (A) Total absorbance raw average spectra of the large-diameter DRG neuron on each IR optical substrate and thermal condition are shown. (B–K) Chemical images derived from large neurons plated on BaF$_2$ substrate and cultured in 4 °C (B–F) and 23 °C (G–K) for O–H & N–H group (B, G), hydrocarbon (C, H), Amide I (D, I), PO^{2-} asymmetric stretching of phosphate (E, J) and C–C and C–O–C stretching of carbon (F, K). (L–S) Chemical images derived from large neurons plated on CaF$_2$ substrate and cultured in 4 °C (L–O) and 23 °C (P–S) for O–H group (L, P), hydrocarbon (M, Q), Amide I (N, R) and PO^{2-} asymmetric stretching of phosphate (O, S). (T–W) Chemical images generated from respective neuron plated on glass substrate and cultured in 4 °C (T–U) and 23 °C (V–W). Scale bar in (B) represents 20 μm and applied to all images.

H stretches and the Amide I bands (Fig. 1 panels B, D respectively) both show a lack of material in the center of the neuron. The images show one main neuron with two partial neurons in the field of view. In Fig. 1 panel A (blue spectrum), the absorption spectrum for this neuron is clearly much less absorbing than the spectra for the other preparation conditions.

CaF$_2$ windows were employed in this study as a well-recognized biocompatible IR substrate with BaF$_2$ window and used to compare the spectral features of the cultured neurons. Chemical images for the LD neurons plated on CaF$_2$ substrate maintained at 23 °C prior to dissociation (Fig. 1 panels P–S) and at 4 °C (Fig. 1 panels L–O) are shown and the chemical distributions for both thermal conditions are normal. The images show one main neuron in the field of view. In Fig. 1 panel A, the absorption spectrum for the LD DRG neuron maintained at 23 °C/4 °C (grey/pink spectrum) and plated on CaF$_2$ window is represented.

Next, consider the results for measured LD neurons, deposited on the BaF$_2$ substrate after the intact DRG was maintained at 23 °C prior to dissociation (Fig. 1 panels G–K). The chemical images are similar to the neurons plated on glass, clearly showing homogeneous chemical distributions for Amide I and N–H/O–H absorption bands, and importantly

different than the images of the neurons that were dissociated from intact DRGs that were exposed to 4 °C. In the present case, only one neuron was in the field of view. Finally, LD neurons prepared at 23 °C and deposited on glass coverslips were also measured, (Fig. 1 panels V–W) and show similar chemical distributions to the other glass substrate sample.

In sum, five sample preparations show normal biological spectra and chemical images within biological variations. Samples prepared from intact DRGs maintained at 4 °C, and then deposited on BaF$_2$ have distinctly different chemical distributions. Also, there is a significant decrease in the intensities of Amide I band at 1650 cm^{-1} and the spectral region 3600–3000 cm^{-1} with respect to the samples prepared on glass (Fig. 1-A; green and black spectrum), CaF$_2$ (Fig. 1-A; grey and pink spectrum) and at 23 °C on BaF$_2$ (Fig. 1-A; red spectrum) while lipid content from C–H functional groups absorb a similar intensity. This is consistent with the chemical images, generated from the distribution of the functional groups based with spectral regions shown in Fig. 1-A. For example, C=O stretching of amide functional groups in protein and O–H functional group, as observed in the images (Fig. 1; panels B, D) show a hole of missing material (consisting of protein and carbohydrate), and what appears to be elevated lipid to the edges of the neurons. Importantly, both the average spectra
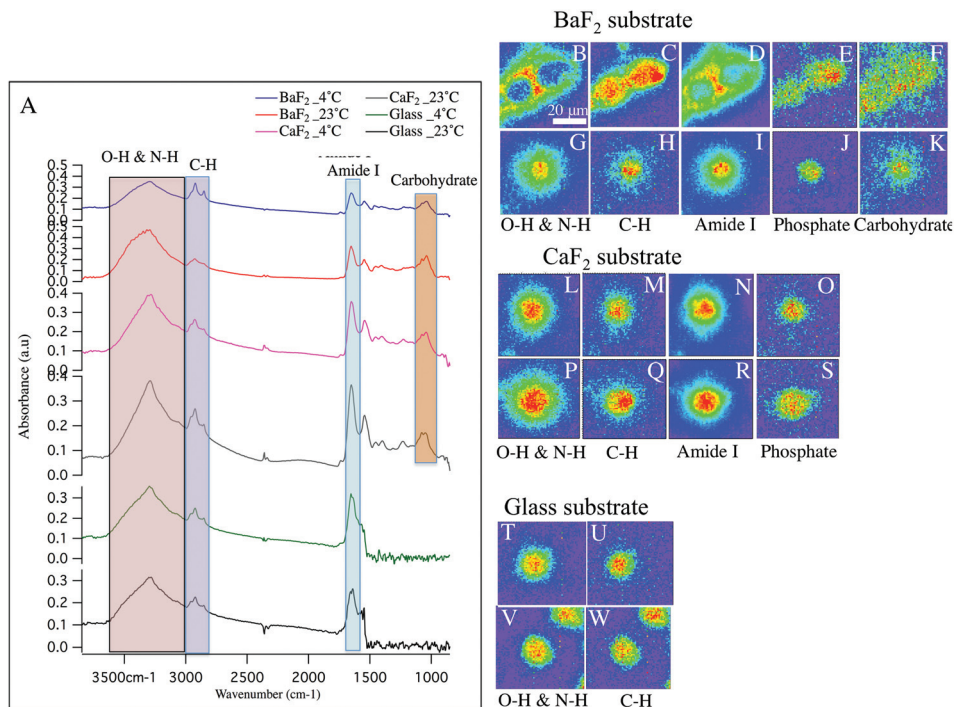
Fig. 2 (A) Total absorbance raw average spectra of the small-diameter DRG neuron on each IR optical substrate and thermal condition are shown. (B–K) Chemical images derived from small neurons plated on BaF$_2$ substrate and cultured in 4 °C (B–F) and 23 °C (G–K) for O–H & N–H group (B, G), hydrocarbon (C, H), Amide I (D, I), PO^{2-} asymmetric stretching of phosphate (E, J) and C–C and C–O–C stretching (F, K). (L–S) Chemical images derived from small neurons plated on CaF$_2$ substrate and cultured in 4 °C (L–O) and 23 °C (P–S) for O–H group (L, P), hydrocarbon (M, Q), Amide I (N, R) and C–C and PO^{2-} asymmetric stretching of phosphate (O, S). (T–W) Chemical images generated from respective neuron plated on glass substrate and cultured in 4 °C (T–U) and 23 °C (V–W). Scale bar in (B) represents 20 μm and applied to all images.

and general trends of the chemical images of neurons plated on glass and CaF$_2$ do not exhibit significant differences.

### Small diameter DRG neurons chemistry and morphology

Fig. 2 shows similar trends as observed in Fig. 1, but for the small diameter sensory neurons. Absorption spectra from small-diameter neurons are plotted in Fig. 2 panel A. Importantly, Comparing the average spectrum from BaF$_2$-4 °C (blue spectrum) and BaF$_2$-23 °C (red spectrum) clearly shows a significant difference. Note, the intensity of PO^{2-} asymmetric stretching band of phosphates in lipids, sugars and nucleic acids, C=O stretching band of amide functional groups in protein and N–H/O–H stretching band are very low in intensity compared to C–H stretching band of hydrocarbons in BaF$_2$-4 °C spectrum (Fig. 2 panel A; blue spectrum). Average spectra from glass-4 °C (green spectrum), glass-23 °C (black spectrum), CaF$_2$-23 °C (grey spectrum), CaF$_2$-4 °C (pink spectrum) and BaF$_2$-23 °C (red spectrum) do not exhibit any significant differences, which is consistent with chemical images. The chemical images of the SD neurons from intact DRGs maintained at 4 °C and plated on BaF$_2$ substrate are shown in Fig. 2 panels B–E. They are in agreement with the results for similarly prepared LD neurons that show missing material for Amide I and N–H/O–H functional groups (Fig. 2 panels B, D). In this case there are two neurons in the field of view. Images

of the SD neurons deposited on glass coverslips from intact DRGs maintained at 4 °C (Fig. 2 panels T–U) and 23 °C (Fig. 2 panels V–W), CaF$_2$ window from intact DRGs maintained at 4 °C (Fig. 2 panels L–O) and 23 °C (Fig. 2 panels P–S) and the neurons plated on BaF$_2$ from intact DRGs at 23 °C (Fig. 2 panels G–K) show normal chemical distributions within the neurons. Chemical images in Fig. 2 panels T–W illustrate one full neuron at the center and a partial neuron in the field of view.

Statistical analysis

The relative lipid content for subpopulations of wild-type naive DRG neurons separated by size (small and large diameter), prepared from three mice, was evaluated. The ratio of the base-lined-corrected area underneath the C–H absorption band to that of the Amide I absorption band for each neuron is calculated as described previously.[33] We employed one-way-ANOVA statistical analysis in order to determine whether there is any significant difference in the relative lipid content within the neurons for any thermal condition (4 °C or 23 °C) or substrate (BaF$_2$, CaF$_2$ and glass coverslip). Results were studied as means ± variations and the relative lipid content for each neuron derived and compared for each thermal condition and any substrate. *P* Values, equal or less than 0.05, were accepted as a significant level of difference between subpopulations of
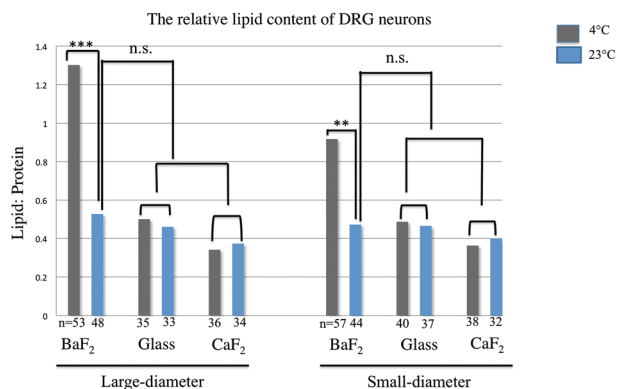
Fig. 3 Relative lipid content for small- and large-diameter neurons from naïve wild-type mice. Relative lipid content significantly increases in small-diameter and large-diameter neurons maintained at 4 °C and plated on BaF$_2$ substrate (***p < 0.001; one-way ANOVA test), whereas there were no significant differences in large-diameter and small-diameter neurons plated on glass coverslip and CaF$_2$ window. n.s. represents no significant difference (*p*-value >0.05) between groups of samples. Also, relative lipid content was not increased in BaF$_2$-23 °C compared to CaF$_2$-4 °C, CaF$_2$-23 °C, glass_23 °C and glass_4 °C and the difference is not significant.

neurons in any condition. This is relevant since this ratio has been previously demonstrated to be sensitive to inflammation[33] and should therefore be a good measure of statistically equivalent chemical condition. Fig. 3 shows a significant increase in the relative lipid content (due to a reduction in the Amide I absorption) in both small-diameter and large-diameter neurons placed on BaF$_2$ window and maintained at 4 °C (*n* = 53 LD and *n* = 57 SD) *versus* 23 °C (*n* = 48 LD and *n* = 44 SD) which is in agreement with our observation from chemical images and IR spectra (*p* < 0.001; one-way ANOVA test). However, there was no significant difference in the relative lipid content of large diameter and small-diameter neurons plated on CaF$_2$ for any thermal condition. 36 LD neurons and 38 SD neurons maintained at 4 °C, and 34 LD neurons and 32 SD neurons maintained at 23 °C, and plated on CaF$_2$ window were used for statistical analysis. Also, there were no significant differences in large-diameter (*n* = 35 at 4 °C and *n* = 33 at 23 °C) and small-diameter neurons (*n* = 40 at 4 °C and *n* = 37 at 23 °C) plated on glass substrate. Importantly, there was no significant difference in the relative lipid content of neurons prepared at 23 °C then deposited on BaF$_2$ substrate and those prepared at either 23 °C or 4 °C and then placed on CaF$_2$ or glass coverslips. Results from statistical analysis are shown in Fig. 3.

Principal component analysis

Principal component analysis (PCA) is used as a discriminating tool to reveal the spectral similarities or differences between different groups of samples. PCA was performed on the mean absorption spectra (*i.e.* vector normalized) for the large diameter and small diameter DRG neurons plated on different substrates (BaF$_2$ and CaF$_2$) resulting in principal

component (PC) scores for each sample. The first three PCs usually have more than 90% of the total variability and therefore PC1 and PC2 were used to construct a 2D scatter plot. Every single point in the scatter plot represents an average spectrum and clusters represent LD and SD neurons from particular sample preparation.

To have a fair comparison between BaF$_2$ and CaF$_2$ substrates, the spectral region 3800–1000 cm^{-1} was used for PCA analysis and it provides the vibrations of the most important functional groups including carbohydrates, protein and lipid. The scatter plots in Fig. 4 panels A, B show that both large diameter and small diameter DRG neurons maintained at 4 °C and plated on BaF$_2$ substrate (red dots) are more diverse than
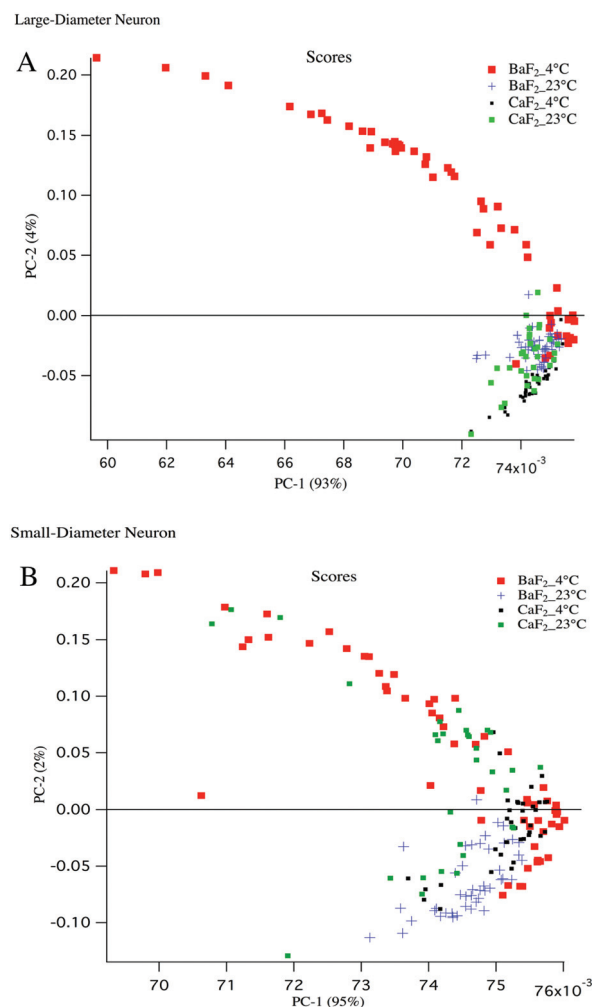
Fig. 4 (A) 2D scatterplot of principal component (PC) scores for large diameter neurons. PC scores for average spectra of the LD neurons (*n* = 53 for BaF$_2$_4 °C, *n* = 48 for BaF$_2$_23 °C, *n* = 36 for CaF$_2$_4 °C and *n* = 34 for CaF$_2$_23 °C) are shown. LD neurons from BaF$_2$_4 °C group have the largest variations (red dots) compared to other clustered groups. (B) PC scores for small diameter neurons (*n* = 57 for BaF$_2$_4 °C, *n* = 44 for BaF$_2$_23 °C, *n* = 37 for CaF$_2$_4 °C and *n* = 32 for CaF$_2$_23 °C) are plotted. Average spectra used for PCA analysis are vector normalized for the mid-IR spectral region 3800–1000 cm^{-1}. SD neurons from BaF$_2$_4 °C group have the largest variations (red dots).

Table 1 Average and standard deviation of PC1 score values for LD and SD neurons maintained at 4 °C and 23 °C and then plated on BaF_2 and CaF_2 substrates are compared. It clearly shows higher distribution variability for the neurons maintained at 4 °C and plated on BaF_2 substrate, which is seen in 2D scatterplot in Fig. 4

PC1 scores	4 °C PC1 mean + S.D.	23 °C PC1 mean + S.D.
BaF_2-LD neurons	0.0715 + 0.0036	0.0745 + 0.000614
BaF_2-SD neurons	0.07425 + 0.0017	0.0746 + 0.00050
CaF_2-LD neurons	0.07433 + 0.000654	0.07425 + 0.00064
CaF_2-SD neurons	0.0751 + 0.000515	0.0744 + 0.000738

the strictly clustered points attributed to the neurons maintained at 23 °C and plated on BaF_2 (blue markers) or CaF_2 (green dots) substrate. It is worth noting that for LD neurons, PC1 accounts for 93% and PC2 accounts for 4% of the total variance, whereas for SD neurons PC1 explains 95% and PC2 only 2% of the total variance. The mean and standard deviation of the PC1 scores for BaF_2 and CaF_2 substrates for LD and SD neurons maintained at each thermal condition is displayed in Table 1. It shows that the neurons maintained at 4 °C and deposited to the BaF_2 substrate have larger variations in PC1 values compared to the neurons maintained at 23 °C which is in agreement with our findings from lipid to protein ratios plotted in Fig. 3. Fig. 4 panel B shows that SD neurons are more heterogeneous and there are more variations for the SD neurons maintained at 23 °C and plated on a CaF_2 substrate in comparison with LD neurons prepared with the same procedure.

### Temperature and substrate-induced effects on DRG neurons

Chemical images, absorption spectra and relative lipid/protein contents in the neurons are used together to compare DRGs dissociated from intact DRGs maintained at different temperatures and plated on different substrates. Measurements from subpopulations of sensory neurons maintained at 4 °C/23 °C and plated on laminin-coated glass coverslips and CaF_2 window revealed normal distributions of the functional groups. Absorption spectra for each thermal condition plotted on the same scale, represent the same intensity for each functional group and correspondingly the relative lipid content is not significantly different for the neurons that are plated on either glass or CaF_2 and prepared under any thermal condition. The glass slides, as predicted, are biocompatible substrates and appropriate for monitoring the changes in N–H, O–H and C–H functional groups *in situ*.

The impact of the BaF_2 substrate seems to be more complex. For DRG sensory neurons that are maintained at 4 °C preceding dissociation, the chemical images and average absorption spectra shown in Fig. 1 panels A, B–F (LD neurons) and Fig. 2 panels A, B–F (SD neurons) show distinct loss of material, both spatially and spectrally, compared to other preparations. The intensities of the Amide I, C–O–C and C–C stretching found in O–H stretches in carbohydrates and N–H

stretches in amides, are significantly reduced relative to the C–H stretching bands. Note that the spectra plotted in Fig. 1 panel A and Fig. 2 panel A are all on the same scale, highlighting functional groups that were depleted in BaF_2-4 °C prepared samples. It appears that protein and water constituents are not present in the somata and most of what remains is a membrane, because these neurons seem to be mostly composed of lipid. Comparing with a normal neuron, the lipid is not elevated; rather everything else is largely depleted, which suggests that the membrane is compromised and the contents of the neuron have leaked out. It is known that dissociated dorsal root ganglia (DRG) neurons quickly become hyperexcitable and these excitatory changes occur rapidly after dissociation.[34] Since some neurons are activated by cold; it is possible that prolonged cold exposure prior to dissociation could be leading to cell damage and ultimately cell lysis.[35] There are numerous studies about the identification of the ion channels that are responsive to cold stimulus in the central nervous system.[35–37] It is possible that the transient receptor potential (TRP) family of ion channels including TRPV4 (known as hypoosmolarity-activated ion channel) or TRPM8, (which is activated by cold[38–40]), or possibly TRPA1 (which some groups have suggested is activated by cold[41,42]), may contribute to this finding. However, it is important to recall this only happens on the BaF_2 substrate, not the glass and CaF_2 substrates, where the spectra and chemical images of the neurons appear similar under both temperature preparation conditions.

Cold shock response, which is a physiological response after rewarming the cell or after a cell has been exposed to cold temperature is potentially responsible for the observations reported here. It is well studied that changes in temperature can induce shock and lead to apoptosis of the cells.[43–46] Infrared signatures of apoptosis are consistent with DNA fragmentation and unraveling.[47] The spectra for the large-diameter (Fig. 5 panel A) and small-diameter (Fig. 5 panel B) neurons that have been exposed to 4 °C (blue spectrum) and 23 °C (red spectrum) for the DRGs plated on BaF_2 window are shown. We found that for the intact DRGs maintained at 4 °C, the infrared band at 1080 cm^{-1}, which has contributions from both the PO^{2-} symmetric stretching mode and the C–O stretching mode of carbohydrates, is diminishing compared to the spectra for the neurons maintained at 23 °C. The peak intensity at 1739 cm^{-1} comes from C=O stretching vibrations of the ester functional groups in lipids, mainly phospholipids in cellular membranes is relatively high in the spectrum for the neurons that were exposed to 4 °C compared to the spectrum for those that were exposed to 23 °C. Moreover, the relative intensity of the bands associated with the symmetric and asymmetric stretching mode of CH_2 (respectively at 2856 cm^{-1} and 2923 cm^{-1}) to the symmetric and asymmetric stretching mode of CH_3 (respectively at 2873 cm^{-1} and 2960 cm^{-1}) is more prominent for the neurons exposed to 4 °C. The relative changes in the bands described here and highlighted in Fig. 5 panels A, B suggest programmed cell death in DRG neurons exposed to 4 °C. It is noteworthy that the infrared bands at 1044, 1177 (±5 cm^{-1}), and 1222 cm^{-1}, which are indicative of DNA frag-
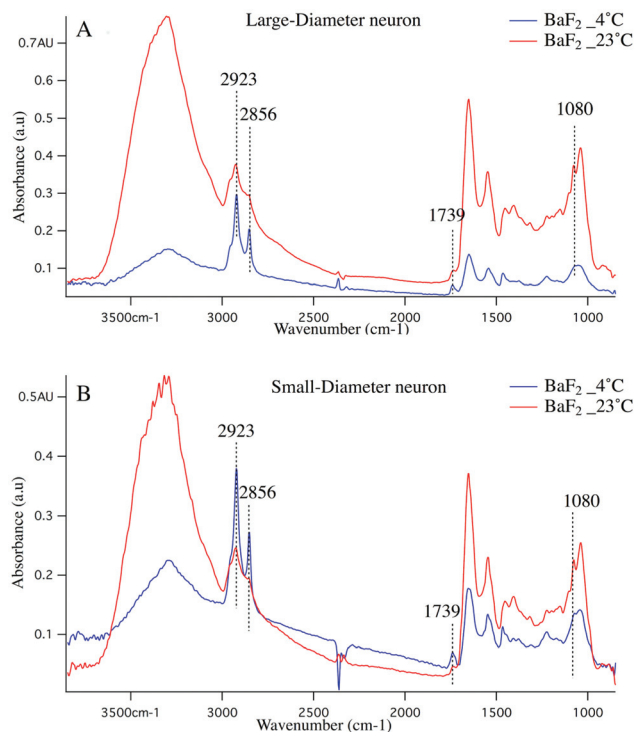
Fig. 5 Absorption spectra of the large diameter (A) and small diameter (B) DRG neurons on BaF_2 substrate are shown. Red (blue) spectrum corresponds to the cells maintained at 23 °C (4 °C) prior to dissociation and plating on BaF_2 substrate. BaF_2_4 °C spectrum (blue spectrum) clearly shows elevated CH_2 bands (highlighted with dotted lines) relative to CH_3 functional group in lipids and everything else is completely depleted. Infrared signatures attributed to apoptosis including a relative decrease at 1080 cm^{-1} and increase in 1739 cm^{-1} are shown and they are more pronounced in small diameter compared to large diameter neurons. BaF_2_23 °C spectrum (red spectrum) depicts normal distributions of functional groups within the cell for both large and small diameter neurons.

mentation, and suggest early stages of apoptosis,[47] are seen in the spectra for both small diameter and large diameter cells maintained at 4 °C. We do not see the relative increase in lipid profile in the glass-plated and CaF_2-plated neurons for any preparation. To highlight finer spectral details, the second derivative spectra of the large diameter (Fig. 6 panels A, B) and small diameter (Fig. 6 panels C, D) neurons plated on all substrates and for all thermal conditions are shown. Second derivative spectra in lipid region for both LD (Fig. 6 panel A) and SD (Fig. 6 panel C) neurons show higher relative lipid content (CH_2/CH_3) for the neurons maintained at 4 °C and plated on BaF_2 substrate (red spectrum) compared to other conditions. Fig. 6 panels B, D show the magnified protein region for LD and SD neurons and it does not demonstrate any shift in Amide I band at 1650 cm^{-1}. Second derivative spectra from the neurons plated on glass substrate (pink and turquoise spectra) are dominated by noise below 1600 cm^{-1}.

Since the substrate has a large influence, we now discuss its potential role. Previous studies of cell growth and morphology

on different optical substrates included viability tests, and revealed that BaF_2 substrates were not always suitable for cell growth due to the chemical toxicity and water solubility.[48] It is possible that ion concentration of the substrate could influence adhered neurons, and cause the neurons to rupture. Osmotic pressure is a parameter that controls the flow of the solvent into the solution through the membrane and is given by the Van't Hoff formula. The formula is $P = CRT$ where P is the osmotic pressure, C is the molar concentration of the solute, $R = 0.082$ (liter bar) (deg mol)$^{-1}$, is the gas constant, and T is the temperature on the absolute temperature scale (Kelvin). We hypothesize that the sensory neurons that are prepared from intact DRGs maintained at 4 °C and then dissociated and plated on BaF_2 windows experience variations in osmotic pressure. Previous studies of artificial membranes identified the relationship between osmotic pressure and ion concentration, mimicking the functions of biomembrane while controlling the osmotic pressure. These studies, using a molecular recognition ion gating membrane, found a response to Ba^{2+} ions that generated an osmotic pressure, whereas Ca^{2+} ions did not initiate the same changes.[49] The thermal responses of a corneal cold receptor were investigated before and after application of Ba^{2+} ion and it shows that Ba^{2+} ions selectively reduced the response of the receptors to heating.[50]

We propose that the intact DRGs exposed to 4 °C experience cold shock that could induce osmotic imbalance due to a gradient in the ionic concentrations across the cell membrane. Recall that these intact DRGs are maintained at 4 °C for between 20–30 minutes after they are dissected from the animal. Then these intact DRGs are removed from the ice bath to dissociate the neurons, which takes 2 hours at 23 °C, and then the neurons are plated on the window. The temperature for this procedure is constant for all sample preparations. Thus, if cold shock induces a change in internal cellular ion concentrations, osmotic imbalance can occur when plated on BaF_2 and eventually lead to osmotic lysis. Apoptosis is not observed for DRGs that are maintained at 23 °C after dissected out of the animal, or for any neurons plated on CaF_2 window and glass. It is plausible that for the neurons maintained at 23 °C, the ions in the substrate that are dissolved in the medium set up an ion potential outside the neuron, but it does not reach the threshold to modify osmotic pressure.

It is worth noting that a larger percentage (44%) of the LD neurons are lysed compared to the SD neurons (31%). The large neurons are known to rupture more easily during the dissociation process due to the larger volume to surface area ratio, whereas membranes in smaller neurons seem tougher and they have lower volume to surface membrane area ratio. Thus, LD neurons are more susceptible to damage. As demonstrated in Fig. 5, highlighted infrared bands associated with unraveling DNA are clearly present in SD neurons, supporting the hypothesis that the cells have initiated apoptosis before they were ruptured.

Another potential contribution to the apparent changes in the cells could be attributed to the laminin coating on the substrates since laminin suppresses the mechanosensitivity
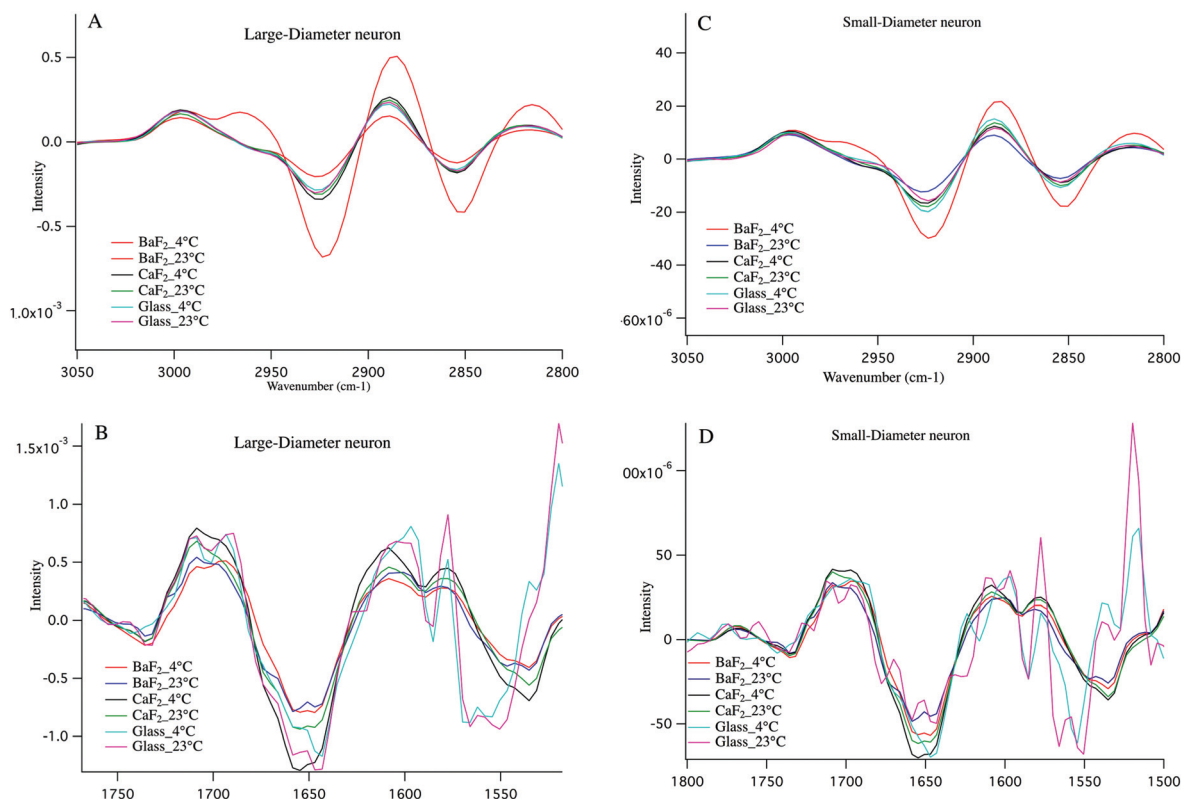
Fig. 6 Second derivative average spectra for large diameter (A, B) and small diameter (C, D) DRG neurons in protein region (B, D) and lipid region (A, C) for BaF_2_4 °C, BaF_2 _23 °C, CaF_2_4 °C, CaF_2_23 °C, glass_4° and glass_23 °C are shown. It clearly shows that the neurons maintained at 4 °C and plated on BaF_2 window has higher intensity in the spectral component associated with lipid, compared to the other conditions.

current in neurons.[51] It has been shown that presence of laminin changes the physical structure of the matrix, leading to the disappearance of a tether protein.[52] However, this was similar for all sample preparations, so it is less likely to be a main contributing factor.

As demonstrated in Fig. 3, for neurons plated on BaF_2 after exposure to 4 °C, the lipid/protein ratio increases significantly which is due to a decrease in protein profile. Importantly, the relative lipid content is not significantly different for neurons that are placed on CaF_2 and glass slides after being prepared under different thermal condition and neurons plated on BaF_2 after being exposed to 23 °C. Prominently, over the entire spectral region, these neurons give rise to a normal chemical distribution for samples plated on BaF_2 and maintained at 23 °C for the entire sample preparation and for both glass and CaF_2 substrates sample preparations. Our findings indicate that both substrate and temperature choices during cell preparation can have consequences in cell maintenance, and specifically impact the results from infrared microscopy.

Conclusions

In this study, we have focused on the effect of sample preparation and substrate choice for chemical imaging of DRG iso-lated neurons, which is important for both the infrared and biomedical community. DRG neurons appeared lysed after the neurons were dissociated from intact DRGs that were dissected and maintained at 4 °C for between 20–30 minutes and plated on BaF_2 infrared transparent window 2 hours later. We have considered several different mechanisms for this response. One possible explanation is related to cold-evoked stimulation of transient receptor potential (TRP) family of ion channels such as Transient Receptor Potential Melastatin 8 (TRPM8), which mediates much of the direct activation of sensory neurons by cold stimuli. However, it is unlikely that TRPM8 mediates the effects we observe given that many large diameter neurons, which do not express TRPM8, were lysed. Instead, it is known that the large neurons are liable to lyse more since they rupture more easily during the typical dissociation process and they are more fragile due to a larger volume to surface area ratio. Since the observation is that only specific dissociated neurons (from the intact DRGs maintained at 4 °C and plated two hours later) plated on salt windows lack protein and carbohydrate content, it is possible that the neurons experience cold shock when maintained at 4 °C, which can initiate many different cellular stress responses leading to apoptosis. It can simply make the neurons more susceptible, however similarly treated neurons are not damaged when plated on CaF_2 and glass substrates.

We suggest that an osmotic imbalance develops when these neurons are plated on the salt substrate. Since the salt substrates have a certain chemical potential for all cell preparations, osmotic lysis could be promoted based on modified ion concentration in the neurons. While we do not have independent verification for ion concentrations, the present results would suggest that the intact DRGs maintained at 4 °C and plated on BaF_2 window might have a modified internal ion concentration as compared to intact DRGs that were maintained at 23 °C. When similar dissociated neurons are plated on either CaF_2 or glass (chemically inert substrate), osmotic imbalance cannot occur and the majority of the neurons are intact. Importantly, the five other conditions that are investigated in this study, namely BaF_2-23 °C, CaF_2-4 °C, CaF_2-23 °C, glass-4 °C, glass-23 °C give rise to the normal results, within biological variation, providing the evidence that DRGs can be successfully plated on BaF_2 windows for mid-IR specific chemical imaging.

Abbreviations

IR	Infrared
BaF_2	Barium fluoride
CaF_2	Calcium fluoride
DRG	Dorsal root ganglion
LD	Large-diameter
SD	Small-diameter
TRPV4	Transient receptor potential subfamily V member 4
TRPM8	Transient receptor potential subfamily M member 8
TRPA1	Transient receptor potential Ankryn 1

Acknowledgements

Notes and references

1 A. I. Basbaum, D. M. Bautista, G. Scherrer and D. Julius, *Cell*, 2009, **139**, 267–284.

2 E. A. Lumpkin and M. J. Caterina, Mechanisms of sensory transduction in the skin, *Nature*, 2007, **445**, 858–865.

3 E. Gascon and A. Moqrich, Heterogeneity in Primary Nociceptive Neurons: From Molecules to Pathology, *Arch. Pharmacal Res.*, 2010, **33**, 1489–1507.

4 C. E. Le Pichon and A. T. Chesler, The functional and anatomical dissection of somatosensory subpopulations using mouse genetics, *Front. Neuroanat.*, 2014, **8**, 00021.

5 V. E. Abraira and D. D. Ginty, The Sensory Neurons of Touch, *Neuron*, 2013, **79**, 618–639.

6 M. J. Zylka, F. L. Rice and D. J. Anderson, Topographically distinct epidermal nociceptive circuits revealed by axonal tracers targeted to Mrgprd, *Neuron*, 2005, **45**, 17–25.

7 A. E. Dubin and A. Patapoutian, Nociceptors: the sensors of the pain pathway, *J. Clin. Invest.*, 2010, **120**, 3760–3772.

8 J. Hjerling-Leffler, M. AlQatari, P. Ernfors and M. Koltzenburg, Emergence of functional sensory subtypes as defined by transient receptor potential channel expression, *J. Neurosci.*, 2007, **27**, 2435–2443.

9 B. J. Zuchero, *Cold Spring Harbor Protoc.*, 2014, **8**, 813–838.

10 E. A. Lumpkin and D. M. Bautista, *Curr. Opin. Neurobiol.*, 2005, **15**, 382–388.

11 S. Dirajlal, L. E. Pauers and C. L. Stucky, *J. Neurophysiol.*, 2003, **89**, 513–524.

12 S. N. Lawson and P. J. Waddell, *J. Physiol.*, 1991, **435**, 41–63.

13 S. N. Lawson, M. J. Perry, E. Prabhakar and P. W. McCarthy, *Brain Res. Bull.*, 1993, **30**, 239–243.

14 O. H. Uhtaek, *et al.*, *The nociceptive membrane*, 2006, vol. 57, ISBN-13:978-0121533571.

15 L. S. Loken, J. Wessberg, I. Morrison, F. McGlone and H. Olausson, *Nat. Neurosci.*, 2009, **12**, 547–548.

16 M. J. Nasse, M. J. Walsh, E. C. Mattson, R. Reininger, A. Kajdacsy-Balla, V. Macias, R. Bhargava and C. J. Hirschmugl, *Nat. Methods*, 2011, **8**, 413–U458.

17 A. M. Nelson, K. L. Marshall and E. A. Lumpkin, *Neuron*, 2011, **71**, 763–765.

18 J. T. Ferraro, M. Daneshmand, R. Bizios and V. Rizzo, *Am. J. Physiol.: Cell Physiol.*, 2004, **286**, C831–C839.

19 Y. Xing, Y. Gu, L.-C. Xu, C. A. Siedlecki, H. J. Donahue and J. You, *J. Cell. Physiol.*, 2011, **226**, 2350–2359.

20 Y. Wang, B. S. Maciejewski, D. Drouillard, M. Santos, M. A. Hokenson, R. L. Hawwa, Z. Huang and J. Sanchez-Esteban, *Am. J. Physiol.: Lung Cell. Mol. Physiol.*, 2010, **298**, 775–783.

21 V. Vasquez, M. Krieg, D. Lockhead and M. B. Goodman, *Cell Reports*, 2014, **6**, 70–80.

22 G. L. Carr, *Rev. Sci. Instrum.*, 2001, **72**, 1613–1619.

23 M. J. Baker, J. Trevisan, P. Bassan, R. Bhargava, H. J. Butler, K. M. Dorling, P. R. Fielden, S. W. Fogarty, N. J. Fullwood, K. A. Heys, C. Hughes, P. Lasch, P. L. Martin-Hirsch, B. Obinaju, G. D. Sockalingum, J. Sule-Suso, R. J. Strong, M. J. Walsh, B. R. Wood, P. Gardner and F. L. Martin, *Nat. Protoc.*, 2014, **9**, 1771–1791.

24 P. Bassan, J. Lee, A. Sachdeva, J. Pissardini, K. M. Dorling, J. S. Fletcher, A. Henderson and P. Gardner, *Analyst*, 2013, **138**, 144–157.

25 J. Filik, M. D. Frogley, J. K. Pijanka, K. Wehbe and G. Cinque, *Analyst*, 2012, **137**, 853–861.

26 K. Y. Kwan, A. J. Allchorne, M. A. Vollrath, A. P. Christensen, D. S. Zhang, C. J. Woolf and D. P. Corey, *Neuron*, 2006, **50**, 277–289.

27 M. E. Barabas, E. A. Kossyreva and C. L. Stucky, *PLoS One*, 2012, 7.

28 M. E. Barabas and C. L. Stucky, *Mol. Pain*, 2013, **9**, 9.

29 S. D. Skaper, Springer Protocols, *Methods Mol. Biol.*, 2012, 846.

30 D. Vilceanu, P. Honore, Q. H. Hogan and C. L. Stucky, *J. Pain*, 2010, **11**, 588–599.

31 D. Vilceanu and C. L. Stucky, *PLoS One*, 2010, **5**, e12177.

32 E. C. Mattson, M. J. Nasse, M. Rak, K. M. Gough and C. J. Hirschmugl, *Anal. Chem.*, 2012, **84**, 6173–6180.

33 M. E. Barabas, E. C. Mattson, E. Aboualizadeh, C. J. Hirschmugl and C. L. Stucky, Chemical Structure and Morphology of Dorsal Root Ganglion Neurons from Naive and Inflamed Mice, *J. Biol. Chem.*, 2014, **289**, 34241–34249.

34 R. H. LaMotte, *J. Neurophysiol.*, 2007, **97**, 1–2.

35 C. Belmonte, J. A. Brock and F. Viana, *Exp. Brain Res.*, 2009, **196**, 13–30.

36 H. H. Andersen, R. V. Olsen, H. G. Moller, P. W. Eskelund, P. Gazerani and L. Arendt-Nielsen, *Eur. J. Pain*, 2014, **18**, 315–325.

37 B. Nilius, G. Appendino and G. Owsianik, *Pflugers Archiv: Eur. J. Physiol.*, 2012, **464**, 425–458.

38 A. D. Gueler, H. Lee, T. Iida, I. Shimizu, M. Tominaga and M. Caterina, *J. Neurosci.*, 2002, **22**, 6408–6414.

39 D. D. McKemy, W. M. Neuhausser and D. Julius, *Nature*, 2002, **416**, 52–58.

40 G. M. Story, A. M. Peier, A. J. Reeve, S. R. Eid, J. Mosbacher, T. R. Hricik, T. J. Earley, A. C. Hergarden, D. A. Andersson, S. W. Hwang, P. McIntyre, T. Jegla, S. Bevan and A. Patapoutian, *Cell*, 2003, **112**, 819–829.

41 D. D. McKemy, *ACS Chem. Neurosci.*, 2013, **4**, 238–247.

42 Y. Karashima, K. Talavera, W. Everaerts, A. Janssens, K. Y. Kwan, R. Vennekens, B. Nilius and T. Voets, *Proc. Natl. Acad. Sci. U. S. A.*, 2009, **106**, 1273–1278.

43 K. Jirsova, P. Sodaar, V. Mandys and P. R. Bar, *J. Neurosci. Methods*, 1998, **82**, 233–233.

44 T. Neutelings, C. A. Lambert, B. V. Nusgens and A. C. Colige, *PLoS One*, 2013, 8.

45 J. H. Fransen, J. W. Dieker, L. B. Hilbrands, J. H. Berden and J. van der Vlag, *Apoptosis*, 2011, **16**, 86.

46 B. L. Soloff, W. A. Nagle, A. J. Moss Jr., K. J. Henle and J. T. Crawford, *Biochem. Biophys. Res. Commun.*, 1987, **145**, 876–883.

47 N. Jamin, L. Miller, J. Moncuit, W. H. Fridman, P. Dumas and J. L. Teillaud, *Biopolymers*, 2003, **72**, 366–373.

48 K. Wehbe, J. Filik, M. D. Frogley and G. Cinque, *Anal. Bioanal. Chem.*, 2013, **405**, 1311–1324.

49 T. Ito and T. Yamaguchi, *J. Am. Chem. Soc.*, 2004, **126**, 6202–6203.

50 J. Brock, M. C. Acosta, A. Al Abed, S. Pianova and C. Belmonte, *J. Physiol.*, 2006, **575**, 573–581.

51 L. Y. Chiang, K. Poole, B. E. Oliveira, N. Duarte, Y. A. B. Sierra, L. Bruckner-Tuderman, M. Koch, J. Hu and G. R. Lewin, *Nat. Neurosci.*, 2011, **14**, 993–U979.

52 J. Hu, L.-Y. Chiang, M. Koch and G. R. Lewin, *EMBO J.*, 2010, **29**, 855–867.